International Scientific Conference 20 UNITECH 26

INTERNATIONAL SCIENTIFIC CONFERENCE
19-21 November 2026
GABROVO

LOAD ANALYSIS OF METALLIC MATERIALS USING UPPERBOUND METHOD

Kaan Ozel

Trakya University, Faculty of Engineering, Department of Mechanical Engineering, Edirne, Turkey

……
**Corresponding author: kaanozel@trakya.edu.tr*

Abstract

In metal forming industry, upsetting is one the important process for production. Upsetting increases the diameters of the workpieces; a material flow occurs and strengthens the parts while shortening their lengths. Friction conditions between metallic materials and molds affects the material flow. Some of the examples for parts produced with upsetting are engine valves, bolts, screws and couplings. In addition, upsetting forces are closely related to geometric shapes of metallic materials that changes the deformation rates.
In this study; load analysis of metallic materials for upsetting different profiles were investigated. The upper bound method was applied; force-stroke diagrams were obtained by the investigation of deformation energy and friction losses. The analyzed parts were prismatic specimen with arbitrary profiles and the results obtained were supported by graphics.

Keywords: Upsetting, Upperbound Method, Metallic Materials, Arbitrary Profiles

INTRODUCTION

Metal plastic forming is a long-standing and widely utilized manufacturing process based on altering the shape of metals through force and pressure without changing their volume. As one of the most prevalent metal forming techniques, upsetting is particularly effective when applied to ductile materials, which can be easily deformed and shaped.
Fundamentally, upsetting involves applying an axial compressive force to a workpiece, thereby reducing its length while simultaneously expanding its cross-sectional area perpendicular to the force direction. Although the overall volume remains constant throughout the process, the induced strain can lead to geometric alterations in the material. For cylindrical parts, this deformation is typically quantified as the upsetting ratio, measured by the percentage reduction in length.

Conducting a thorough force analysis prior to the upsetting process is critical to preventing unexpected failures and manufacturing defects. To achieve an accurate analysis, the punch force (stamp force) must be calculated as a function of the upsetting rate. Among the various mathematical approaches available for this calculation, the upper bound method (upper limit method) is widely preferred, especially for workpieces defined in cylindrical coordinates. This method primarily relies on the upsetting ratio and the relevant friction coefficients.
An investigation into the extrusion of polygonal components using curvilinear profile dies was conducted by Gunasekera and Hoshino (1985). Their findings indicated that curvilinear geometries significantly optimize material flow, thereby enhancing the forming operation. Utilizing the upper bound method, the researchers

This is an open access article licensed under Creative Commons Attribution 4.0 International
Print ISSN: 1313-230X, Online ISSN: 3033-1404

analyzed both curvilinear and linearly tapering dies under specific process parameters, namely a 60% extrusion ratio and a friction factor of 0.1, to derive comprehensive solution graphs. [1]

In their research, Yang, D.Y., et al. (1986) highlighted the mathematical complexities involved in analytically defining die surfaces that connect inlet and outlet sections with distinct profiles using standard cylindrical coordinates. To address this challenge, the study introduces a novel spatial transition function, $R(\theta,z)$, which effectively bridges the inlet profile $R(\theta,0)$ and the outlet profile $R(\theta,L)$. Developed through a specific number of Fourier series, this transition function successfully defines the inlet geometry at $z=0$ and the outlet geometry at $z=L$. By leveraging this mathematical framework, the authors formulated a new velocity field model. To validate their approach, the theoretical outcomes for both elliptical and rectangular cross-sectional exit profiles were evaluated via the upper bound method and compared against empirical data obtained from experimental trials using Al 2024 aluminum alloy. [2]

A novel approach combining the slab and upper-bound methods was proposed by Bakhshi-Jooybari, M. et al. (2007) to evaluate the forming load in the cold extrusion of aluminum and lead specimens. To benchmark the performance of this hybrid analytical framework, the authors utilized previously designed conical dies for comparative analysis. The theoretical predictions generated by the proposed method were rigorously validated against both empirical data and numerical solutions obtained from commercial Finite Element Method (FEM) software. The resulting experimental force-stroke diagrams demonstrated that the integrated slab-upper bound approach exhibits strong correlation and compatibility with both the simulation models and the experimental outcomes. [3]

A novel design and analytical methodology were developed by Abrinia, K. and Makaremi, M. (2009) to model material flow through expanding square, rectangular, and elliptical cross-sections. The selected dies were specifically engineered to guide material flow toward the lateral surfaces. The researchers investigated dies featuring various extrusion ratios to evaluate the influence of process parameters—such as friction and extrusion ratio—on the required extrusion pressure. While the upper bound analysis method was utilized to determine the maximum extrusion pressure, the finite element method (FEM) was preferred to facilitate and optimize the die design process. [4]

In forging, a fundamentally simple initial part, such as a billet, undergoes plastic deformation between two dies to achieve the target geometry. Upsetting and open-die forging represent highly significant processes within the field of metal forming. During these operations, interfacial friction conditions between the specimen and the die exert a more pronounced influence on material flow and stress distribution than temperature and strain rates. The friction coefficient escalates in specimens exhibiting a high diameter-to-height ratio, which subsequently triggers barreling during upsetting. As illustrated in Figure 1, under ideal (frictionless) conditions, a cylindrical specimen with an initial height of h_0 and diameter of d_0 homogeneously deforms to a final height of h_1 and a corresponding diameter of d_1. In practice, however, material flow toward the die faces is restricted at the contact interfaces due to friction and thermal chilling, thereby inducing the barreling phenomenon.

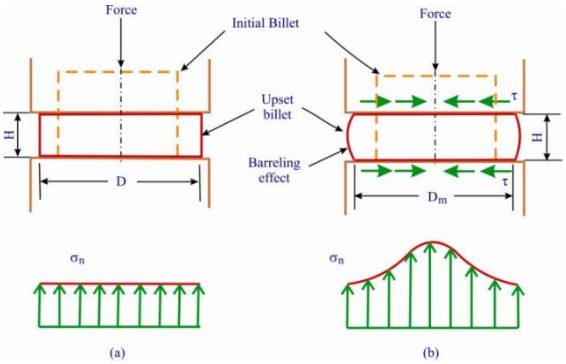


Fig. 1. *Schematic illustration of upsetting process*

ANALYTICAL INVESTIGATION

In this study; load analysis of metallic materials for upsetting elliptical prismatic specimen with arbitrary profiles were investigated. The upper bound method was applied; force-stroke diagrams were obtained by the investigation of deformation energy and friction losses.

Upper Bound Analysis Method

To determine the total power consumption within the framework of the upper bound method, all energy dissipations must be comprehensively accounted for. The cumulative power consumption is derived by individually computing the energy consumed across each distinct process, thereby establishing the upper limit for the total power required.

J^*: Upper bound for total power consumption

$$J^* = \sum \dot{W}_t + \sum \dot{W}_s + \sum \dot{W}_f \quad (1)$$

$\dot{W}_i$: Ideal deformation power

$$\dot{W}_i = \bar{\sigma}_m^{(l)} \int \dot{\bar{\varepsilon}}\, dV \quad (2)$$

$\dot{\bar{\varepsilon}}$: Effective strain velocity

$$\dot{\bar{\varepsilon}} = \frac{2}{\sqrt{3}}\left(\frac{1}{2}\left(\dot{\varepsilon}_r^2 + \dot{\varepsilon}_\theta^2 + \dot{\varepsilon}_z^2\right) + \dot{\varepsilon}_{r\theta}^2 + \dot{\varepsilon}_{\theta z}^2 + \dot{\varepsilon}_{zr}^2\right)^{1/2} \quad (3)$$

$\bar{\sigma}_m^{(j)}$: Effective stress value

$$\bar{\sigma}_m^{(j)} = \frac{1}{\bar{\varepsilon}_f^{(j)}} \int_0^{\bar{\varepsilon}_f^{(j)}} \sigma d\varepsilon \quad (4)$$

$\bar{\varepsilon}_f^{(j)}$: Effective strain value

$$\bar{\varepsilon}_f^{(j)} = \sum_{i=1}^{j} \ln\left(\frac{H^{(i)}}{H^{(i-1)}}\right) \quad (5)$$

$\dot{W}_f$: Friction power between the mold and the part

$$\dot{W}_f = \frac{m}{\sqrt{3}} \bar{\sigma}_m^{(l)} \int_{S_f} |\Delta V|\, ds \quad (6)$$

P_{avg}: Average stamp pressure

$$P_{avg} = \frac{J^*}{A_r U_0} \quad (7)$$

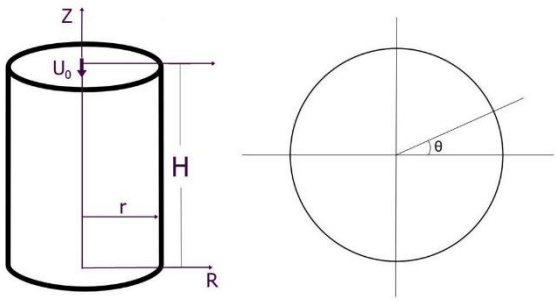


Fig. 2. *Cylindrical coordinates of upsetting*

Kinematic Velocity Elements

For an object defined in cylindrical coordinates, the corresponding velocity components are sequentially designated as U_z, U_θ, U_r with their respective mathematical expressions formulated as follows:

U_z: Axial velocity equation

$$U_z = \frac{-U_0 Z}{T} \quad (8)$$

U_θ: Tangential velocity equation

$$U_\theta = \frac{-U_0 R}{T} \omega_1(\theta) \quad (9)$$

$$\omega_1(\theta) = \frac{(a-b)}{(a+b)} D_1 \sin(2\theta) \quad (10)$$

$$\omega_1(\theta) = \frac{(a-a)}{(a+a)} D_1 \sin(2\theta) = 0 \quad (11)$$

$$U_\theta = \frac{-U_0 R}{T} \omega_1(\theta) = \frac{-U_0 R}{T} . 0 = 0 \quad (12)$$

$$U_\theta = 0 \quad (13)$$

U_r: Radial velocity equation

$$U_r = \frac{U_0 R}{2T} . \left(1 + \frac{d\omega_1(\theta)}{d\theta}\right) \quad (14)$$

$$U_r = \frac{U_0 R}{2T} . (1 + 0) = \frac{U_0 R}{2T} \quad (15)$$

$$U_r = \frac{U_0 R}{2T} \quad (16)$$

Force Analysis for Elliptical Prism

In a similar manner to the calculations executed for the cylindrical part, the governing mathematical equations for the velocity fields of an elliptical material are defined below:

$$U_z = \frac{-U_0 Z}{T} \tag{17}$$

$$U_\theta = \frac{-U_0 R}{T}\omega_1(\theta) \tag{18}$$

$$\omega_1(\theta) = \frac{(a-b)}{(a+b)} D_1\, sin(2\theta) \tag{19}$$

$$\omega_1(\theta) = \frac{(a-b)}{(a+a)} D_1\, sin(2\theta) \tag{20}$$

$$U_\theta = \frac{-U_0 R}{T}\omega_1(\theta) = \frac{-U_0 R}{T}\frac{(a-b)}{(a+a)} D_1\, sin(2\theta) \tag{21}$$

$$U_r = \frac{U_0 R}{2T}.(1 + \frac{d\omega_1(\theta)}{d\theta}) \tag{22}$$

$$U_t = \frac{U_0 R}{2T}(1 + 2\ \frac{(a-b)}{(a+b)} D_1\, cos(2\theta) \tag{23}$$

Based on the principle of volume constancy, the strain rates are expressed by the following equations:

$$\frac{\partial U_r}{\partial R} + \frac{U_r}{R} + \frac{1}{R}\frac{\partial U_\theta}{\partial \theta} + \frac{\partial U_z}{\partial Z} = 0 \tag{24}$$

$$\dot{\varepsilon}_r = \frac{\partial U_r}{\partial R} \tag{25}$$

$$\dot{\varepsilon}_r = \frac{\partial U_t}{\partial R} = \frac{U_0}{2T} + \frac{U_0}{T}\frac{(a-b)}{(a+b)} D_1\, cos(2\theta) \tag{26}$$

$$\dot{\varepsilon}_\theta = \frac{U_r}{R} + \frac{1}{R}\frac{\partial U_\theta}{\partial \theta} \tag{27}$$

$$\dot{\varepsilon}_\theta = \frac{U_r}{R} + \frac{1}{R}\frac{\partial U_\theta}{\partial \theta} = \frac{U_0}{T}(1 + 2\frac{(a-b)}{(a+b)} D_1\, cos(2\theta) + \frac{1}{R}(-2\frac{U_0 R}{T}\frac{(a-b)}{(a+b)} D_1\, cos(2\theta) \tag{28}$$

$$\dot{\varepsilon}_\theta = \frac{U_0}{2T} - \frac{U_0}{T}\frac{(a-b)}{(a+b)} D_1\, cos(2\theta) \tag{29}$$

$$\dot{\varepsilon}_z = \frac{\partial U_z}{\partial Z} \tag{30}$$

$$\dot{\varepsilon}_z = \frac{\partial U_z}{\partial Z} = -\frac{U_0}{T} \tag{31}$$

$$\dot{\varepsilon}_z = -\frac{U_0}{T} \tag{32}$$

The mathematical formulations for the shear strain velocity elements are expressed as follows:

$$\dot{\varepsilon}_{r\theta} = \frac{1}{2}\left(\frac{1}{R}.\frac{\partial U_r}{\partial \theta} + \frac{\partial U_\theta}{\partial R} - \frac{U_0}{R}\right) \tag{33}$$

$$\dot{\varepsilon}_{r\theta} = \frac{1}{2}\left(\frac{1}{R}.\frac{\partial U_r}{\partial \theta} + \frac{\partial U_\theta}{\partial R} - \frac{U_0}{R}\right) = \frac{U_0}{4T} - \frac{U_0}{T}\frac{(a-b)}{(a+b)} D_1\, sin(2\theta) \tag{34}$$

$$\dot{\varepsilon}_{r\theta} = \frac{U_0}{4T} - \frac{U_0}{T}\frac{(a-b)}{(a+b)} D_1\, sin(2\theta) \tag{35}$$

$$\dot{\varepsilon}_{\theta z} = \frac{1}{2}\left(\frac{\partial U_\theta}{\partial Z} + \frac{1}{R}.\frac{\partial U_z}{\partial \theta}\right) \tag{36}$$

$$\dot{\varepsilon}_{\theta z} = \frac{1}{2}\left(\frac{\partial U_\theta}{\partial Z} + \frac{1}{R}.\frac{\partial U_z}{\partial \theta}\right) = \frac{1}{2}\left(0 + \frac{1}{R}.0\right) = 0 \tag{37}$$

$$\dot{\varepsilon}_{\theta z} = 0 \tag{38}$$

$$\dot{\varepsilon}_{rz} = \frac{1}{2}\left(\frac{\partial U_z}{\partial R} + \frac{\partial U_r}{\partial Z}\right) \tag{39}$$

$$\dot{\varepsilon}_{rz} = \frac{1}{2}\left(\frac{\partial U_z}{\partial R} + \frac{\partial U_r}{\partial Z}\right) = \frac{1}{2}(0 + 0) = 0 \tag{40}$$

$$\dot{\varepsilon}_{rz} = 0 \tag{41}$$

The total power consumption is:

$$J^* = \sum \dot{W}_l + \sum \dot{W}_s + \sum \dot{W}_f \tag{42}$$

$$\dot{W}_l = \bar{\sigma}_m^{(j)} \int \dot{\bar{\varepsilon}}\, dV \tag{43}$$

$$\dot{\bar{\varepsilon}} = \frac{2}{\sqrt{3}}(\frac{1}{2}(\dot{\varepsilon}_r^2 + \dot{\varepsilon}_\theta^2 + \dot{\varepsilon}_z^2) + \dot{\varepsilon}_{r\theta}^2 + \dot{\varepsilon}_{\theta z}^2 + \dot{\varepsilon}_{zr}^2)^{1/2} \tag{44}$$

$$\dot{W}_l = \bar{\sigma}_m^{(j)} \int_V \dot{\bar{\varepsilon}}\, dV = \bar{\sigma} \iiint \frac{2}{3}(\sqrt{\frac{1}{2}}(\dot{\varepsilon}_r^2 + \dot{\varepsilon}_\theta^2 + \dot{\varepsilon}_z^2) + \dot{\varepsilon}_{r\theta}^2 + \dot{\varepsilon}_{\theta z}^2 + \dot{\varepsilon}_{zr}^2)\, r dr\, d\theta\, dz) \tag{45}$$

$$\dot{W}_f = \frac{m}{\sqrt{3}}\bar{\sigma}_m^{(l)} \int_{S_f} |\Delta V|\, ds \tag{46}$$

$$\dot{W}_f = \frac{m}{\sqrt{3}}\bar{\sigma}_m^{(l)} \int_{S_f} |\Delta V|\, ds = \frac{m}{\sqrt{3}}\bar{\sigma} \iint \sqrt{U_r^2 + U_\theta^2}\, r dr\, d\theta \tag{47}$$

$$\dot{W}_s = 0 \tag{48}$$

$$J^* = \sum \dot{W}_i + \sum \dot{W}_s + \sum \dot{W}_f = \dot{W}_i + \dot{W}_f \quad (49)$$

$$J^* = Force * Velocity \quad (50)$$

$$F = Area * Pressure \quad (51)$$

Calculations and Results

The theoretical calculations have been established in the equations presented above. In the subsequent stage, dimensional variations will be quantified, and the corresponding results will be analyzed. As illustrated in the figure below, the semi-major and semi-minor axes of the ellipse are designated as "a" and "b", respectively. The pre-process dimensions of the elliptical component are denoted as "a_1" and "b_1", whereas the post-process dimensions are designated as "a_2" and "b_2".

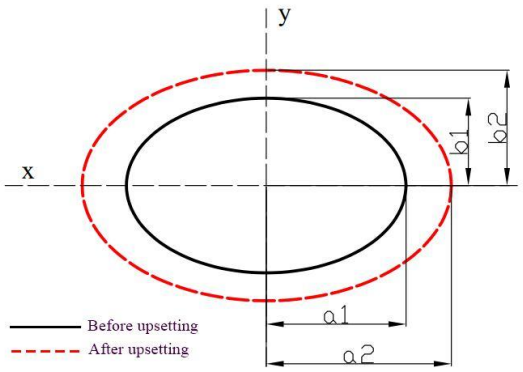


Fig. 3. *Pre-upsetting and post-upsetting surface variations of an elliptical part*

$$\frac{a}{b} = \lambda = \frac{a_1}{b_1} = \frac{a_2}{b_2} \quad (52)$$

$$V = \pi . a . b . h \quad (53)$$

$$V = \pi . a . b . h = \pi . a_1 . b_1 . h_1 = \pi . a_2 . b_2 . h_2 \quad (54)$$

$$b_2 = \sqrt{\frac{a_1 . b_1 . h_1}{h_2 . \lambda}} \quad (55)$$

CONCLUSION

The computed quantitative values reflecting the geometric dimensional changes across various upsetting ratios are systematically presented in Tables 1–3. A comprehensive evaluation of these numerical results indicates that although the height reduction rates remain perfectly identical across all experimental cases, the resulting final dimensions - specifically the major axis (a_2) and the minor axis (b_2) - exhibit a non-uniform variation that depends directly on the initial profile asymmetry coefficient (λ). Specifically, while the final minor axis (b_2) displays a highly consistent and uniform expansion trend regardless of the initial magnitude of λ, the final major axis (a_2) demonstrates a distinct variation that is heavily dictated by the initial aspect ratio of the elliptical cross-section. This highly asymmetric deformation behavior is driven primarily by the differential material flow rates along the orthogonal axes of the ellipse, combined with the frictional shear stress generated at the die-material interface, which imposes non-isotropic boundary constraints on the radial expansion of the specimen.

Table 1. *Lengths obtained with λ = 1,2*

λ = 1,2 for Elliptical Profile					
a_1	b_1	h_1	h_2	b_2	a_2
36	30	24	24	30,0000	36,0000
36	30	24	20	32,8634	39,4360
36	30	24	18	34,6410	41,5692
36	30	24	16	36,7423	44,0908
36	30	24	14	39,2792	47,1351
36	30	24	12	42,4264	50,9117
36	30	24	10	46,4758	55,7710

Table 2. *Lengths obtained with λ = 1,3*

λ = 1,3 for Elliptical Profile					
a_1	b_1	h_1	h_2	b_2	a_2
39	30	24	24	30,0000	39,0000
39	30	24	20	32,8634	42,7224
39	30	24	18	34,6410	45,0333
39	30	24	16	36,7423	47,7650
39	30	24	14	39,2792	51,0630
39	30	24	12	42,4264	55,1543
39	30	24	10	46,4758	60,4185

Table 3. *Lengths obtained with λ = 1,4*

λ = 1,4 for Elliptical Profile					
a_1	b_1	h_1	h_2	b_2	a_2
42	30	24	24	30,0000	42,0000
42	30	24	20	32,8634	46,0087
42	30	24	18	34,6410	48,4974
42	30	24	16	36,7423	51,4393
42	30	24	14	39,2792	54,9909
42	30	24	12	42,4264	59,3970
42	30	24	10	46,4758	65,0661

REFERENCE

[1] J.S. Gunasekera, S. Hoshino, 1985, Analysis of Extrusion of Polygonal Sections Through Streamlined Dies, Journal of Engineering Technology, 107: 229-233.

[2] D.Y. Yang, C.H. Han, M.U. Kim, 1986, A Generalized Method for Analysis of Three-Dimensional Extrusion of Arbitrarily-Shaped Sections, International Journal of Mechanical Sciences, 28: 517-534.

[3] M. Bakhshi-Jooybari, M. Saboori, M. Noorani-Azad, S.J. Hosseinipour, 2007, Combined Upper Bound and Slab Method Finite Element and Experimental Study of Optimal Die Profile in Extrusion, Materials and Design, 28: 229-233.

[4] K., Abrinia, M., Makaremi, 2009, An Analytical Solution for the Spread Extrusion of Shaped Sections, International Journal of Advanced Manufacturing Technology, 41: 670-676.

[5] C.H., Liu, A. C., Wang, Y.S., Chen, C.M., Wang, 2008, The Coupled Thermo-Mechanical Analysis in the Upsetting Process by the Dynamic FEM, Journal of Materials Processing Technology, 201: 37-42.

[6] Ö., Ayer, K., Özel, F., Karaçam, 2011, Load Analysis of Upsetting on Prismatic Specimen with Arbitrary Profiles, UNITECH 2011, International Scientific Conference, Gabrovo, Bulgaria, Vol. 2, November 18-19, 201-204.